Comparative Exergy Analysis of Green Ammonia Production Pathways

Ingrid Rossilho Casale[a]*, Flávia Mendes de Almeida Collaço[b], Carlos Eduardo Keutenedjian Mady[a]

[a]Institute of Energy and Environment, University of São Paulo, São Paulo, SP, Brazil
[b]São Carlos School of Engineering, University of São Paulo, São Carlos, SP, Brazil
**Corresponding Author: ingridrcasale@usp.br*

Abstract:

Ammonia is among the most widely produced chemicals worldwide and plays a fundamental role in the global economy. However, conventional ammonia production is highly energy-intensive and contributes to global warming emissions. In the context of the energy transition and the pursuit of carbon neutrality, the production of green ammonia from renewable energy sources has attracted growing attention. In addition to its importance in agriculture, ammonia is considered a promising energy carrier and hydrogen storage vector, due to transportation challenges. In this context, this work performs a comprehensive exergy analysis of green ammonia production. Different technological routes were evaluated to determine the exergy efficiencies and electrical energy consumption of the proposed configurations, thereby identifying the most suitable alternative from a thermodynamic perspective. The hypothetical plant includes seawater desalination processes using reverse osmosis (RO) and multi-effect distillation (MED). In sequence, electrolysis technologies such as alkaline (AE), proton exchange membrane (PEM), and solid oxide (SOE) are used for hydrogen production. The process includes nitrogen production from cryogenic air separation (CAS), ammonia production via the Haber–Bosch synthesis (HB), and an offshore wind farm supplying electricity to the system. The results indicate that, among the desalination technologies evaluated, RO presents lower exergy destruction, higher exergy efficiency, and lower electricity consumption. Among the electrolysis technologies, SOE showed the best exergy performance, with higher efficiency, lower exergy destruction, and lower electrical energy consumption. Overall, CAS had the lowest exergy efficiency, followed by RO, SOE, and HB. In terms of electrical energy consumption and destroyed exergy, the processes were ranked in increasing order as RO, CAS, HB, and SOE. Therefore, these results provide thermodynamic insights into green ammonia production pathways; however, factors such as technological maturity, economic feasibility, and resource availability should also be considered when selecting the most suitable route.

Keywords:

Exergy analysis; Green Ammonia; Green Hydrogen; Thermodynamic feasibility.

1. Introduction

Approximately 200 million metric tons of ammonia are produced annually, making it the second-most-produced chemical worldwide, after sulfuric acid [1]. Traditionally, ammonia synthesis consumes between 1% and 2% of global energy and accounts for about 1.4% of global CO_2 emissions, due to its reliance on fossil fuels for hydrogen production [2]. Given growing environmental concerns and the pursuit of carbon neutrality by 2050, sustainable alternatives such as green ammonia via water electrolysis have been studied [3]. Water electrolysis produces green hydrogen from renewable electricity, which can then be used in ammonia synthesis, eliminating methane reforming and reducing carbon emissions [4]. Additionally, hydrogen transport over long distances faces challenges due to its low volumetric energy density, even when compressed. Converting hydrogen into ammonia is a viable solution, as ammonia is essential for nitrogen fertilizers - a crucial agricultural input. It is easier and more economical to transport, can be stored as a liquid at ambient temperature and pressure, and serves as a hydrogen carrier or direct fuel [3,5].

The main technologies for green hydrogen production are water electrolysis, biomass, and photocatalysis. Currently, water electrolysis is the most mature, while biomass is a promising alternative [6,7]. Water electrolysis was the first technology used for carbon-free hydrogen, yet only about 4% of global hydrogen comes from electrolysis [8]. In this process, an electric current splits H_2O into hydrogen (H_2) and oxygen (O_2) with high energy demands [9]. There are four main technologies: alkaline electrolysis (AE), proton exchange membrane electrolysis (PEM), solid oxide electrolysis (SOE), and anion exchange membrane (AEM)

electrolyzers [10]. Only alkaline and PEM have been commercialized; the others show potential but remain under development, with AEM being emerging and less mature [11]. They differ in development stage, electrolyte, charge carrier, operating conditions, and ability to handle intermittent energy sources [12].

Alkaline water electrolysis holds 70% of the market share [6]. It is mature, reliable, safe, and relatively low-cost for large-scale hydrogen production [8,11]. However, its limitations include low current density and restricted low-load capacity due to gas crossover through the separator, which raises explosion risks under critical conditions [11,13]. Concentrated KOH electrolyte, though efficient, is corrosive and operates at low pressure, reducing efficiency [13].

Commercially, PEM electrolyzers are mainly used for small-scale production. Their membrane's low permeability minimizes flammable mixtures [8,13,14]. PEM is safer than alkaline electrolysis, as it avoids caustic electrolytes and has lower environmental impact [15]. Another advantage is stable operation with variable energy sources, enabled by rapid proton transport [8]. PEM offers fast dynamic response, high-pressure operation, high current density, compactness, and cleaner operation [13,16,17]. However, its main obstacle is the high cost of electrocatalysts, making the technology more expensive [8,17]. Also, component durability is limited, and corrosion can compromise cell lifetime, especially under industrial conditions [13].

Solid oxide electrolyzers (SOE), still in R&D, operate at high temperatures using steam instead of liquid water, reducing electrical demand and increasing efficiency [8,11,15]. SOE has lower operating costs and can be integrated with industrial waste heat, favoring hydrogen and chemical production (e.g., methanol, ammonia) [15]. On the other hand, high-temperature operation accelerates material degradation and requires more stable electrolytes, limiting system lifetime [10,15]. SOEs are less suitable for intermittent energy sources, as thermal fluctuations can induce microcracks in the electrolyte, compromising performance and durability [8].

Current water electrolysis technologies require high-purity water. Converting seawater into hydrogen using renewable energy is an alternative given the abundance of saline water [18,19]. Water desalination, essential for this conversion, is classified into thermal and membrane processes [20]. Thermal processes (e.g., distillation) use heat to evaporate water and separate salts. Membrane processes, led by reverse osmosis, mainly use pressure and electrical energy [21,22].

Reverse osmosis (RO) is the most widely used desalination method for seawater and brackish water [23]. RO is a hyperfiltration process that produces potable, low-salt water [24]. It applies pressure above osmotic pressure, forcing water through a semi-permeable membrane that retains salts and impurities [21,25]. RO stands out for its simplicity, robustness, efficiency, low corrosion, reduced metal use, and low installation/operating costs [21,24]. Membrane technology has evolved, improving efficiency, durability, and cost [21,26]. However, challenges include membrane and energy costs (a large portion of operating expenses), frequent cleaning, low chlorine resistance, and short durability [21,24,26].

Multi-Effect Distillation (MED), a thermal method, has recently regained interest, increasing its market share [27]. MED operates in a series of evaporators (“effects”), where saline water undergoes multiple boiling stages. Vapor from one stage heats the next, enabling salt separation [21,23,25]. The key principle is gradual pressure and temperature reduction along with the effects [21,27]. A major advantage of MED is low-temperature operation [23], which minimizes corrosion and scaling, reducing pretreatment needs [21,27]. However, lower temperatures require a larger heat transfer area [21,23]. MED plants are typically designed for large capacities [27]. Though not viable on a small scale, they have low installation/maintenance costs, require little supervision, and operate continuously [20,21].

To obtain nitrogen, air separation uses membrane, cryogenic, absorption, or adsorption technologies. Cryogenic distillation, the first developed and most advanced, is more economical and efficient for large-scale operations, producing high-purity products [1,28]. Cryogenic air distillation obtains high-purity gases and is widely used in industry [29]. Like conventional distillation but at much lower temperatures, it has two thermally integrated columns at different pressures. Nitrogen, more volatile, concentrates at the top; oxygen, with a higher boiling point, remains at the bottom [29,30]. Argon is separated in a third column, where an oxygen-argon stream is processed to obtain high-purity argon [31].

The most widely used ammonia production process, accounting for approximately 85% of total production, is the Haber-Bosch process, in use for over 100 years [1]. Nitrogen (N_2) and hydrogen (H_2) react under high pressure and temperature with a catalyst (mainly iron-based) to form ammonia (NH_3). In the industrial process, gases are compressed, then pass through multiple catalytic beds with intermediate cooling to maximize efficiency. Ammonia is separated by condensation, and unconverted gases are recycled [3,32,33].

Therefore, this work aimed to perform a comprehensive exergy analysis of green ammonia production from seawater desalination, water electrolysis for hydrogen, cryogenic air separation for nitrogen, and Haber-Bosch synthesis, assuming renewable energy supply. Different technological routes were evaluated, including desalination methods (multi-effect distillation and reverse osmosis) and electrolysis types (alkaline, PEM, and SOE). The goal was to quantify exergy efficiencies, destroyed exergy, and electrical energy consumption at each stage. Thus, it was compared the exergy performance of the proposed configurations to determine the most suitable alternative from a thermodynamic perspective for large-scale green ammonia production.

2. Methods

A complete plant was modeled considering the stages of seawater desalination, water electrolysis, cryogenic air separation, and ammonia synthesis. This plant was based on the previous studies of [34]. The green ammonia production plant studied, as shown in Figure 1, begins with Seawater Desalination producing brine and H_2O. The H_2O was then used in Electrolysis to generate H_2, O_2, and purge. Additionally, N_2 was obtained through Cryogenic Air Separation, which produced N_2, O_2, Ar, and waste streams. Thus, ammonia was synthesized through the Haber–Bosch process, with H_2 supplied by electrolysis and N_2 from cryogenic separation. The calculations were based on a production of 1000 t of NH_3 per day. Therefore, the amount of air and seawater required to carry out the other processes in the overall plant was calculated. Furthermore, for all plants, each stream was characterized by exergy (b_i). Equation (1), which considers the physical b_{physical} and chemical (b_{chemical}) contributions, was used to calculate the exergy. Note that $\dot{B} = \dot{n} \cdot b$. In addition, the standard chemical exergy of the components was obtained from [35], and the environmental conditions adopted were 298.15 K and 101.325 kPa.

$$b_i = b_{\text{physical}} + b_{\text{chemical}} = \sum y_i \left(h_i - h_0 - T_0 \cdot (s_i - s_0) + R \cdot T_0 \cdot ln(y_i) + b_{\text{chemical}_i}\right) \quad (1)$$

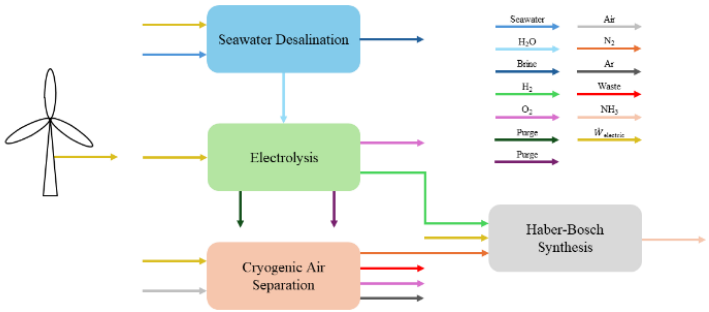

Figure 1. *Schematic representation of the whole plant to produce green ammonia, based on* [34].

2.1. Seawater Desalination

For the desalination of seawater, the processes of reverse osmosis and multi-effect distillation were considered. These technologies were chosen due to their technical and energy advantages compared to other available technologies. MED stands out among thermal processes for presenting higher water and energy efficiency, especially in large-scale applications, while RO stands out among membrane processes due to its greater operational simplicity, lower cost, and wide industrial application. The choice allows a representative comparative evaluation between the two main groups of desalination processes currently used.

2.1.1. Multi-Effect Distillation (MED)

For the Multi-Effect Distillation, the modified six-effect plant of [36] was used, which can be observed in Figure 2. The salinity of seawater was also adopted as the standard value of 35 g/kg, and it was assumed that the water enters and leaves the system at 298.15 K and 101.325 kPa. Mass flow 15 corresponds to 15.25% of flow 24; flow 17 to 31.58%; flow 19 to 48.59%; flow 21 to 65.93%; and flow 23 to 83.17% of flow 24. Mass flows 3, 5, 7, 9, 11, and 12 present identical values and temperatures of 318.15 K. Flow 13 has a pressure of 35.8 kPa and temperature of 384.85 K, while flow 25 has 12.3 kPa and 323.15 K. Flow 26 corresponds to 94.8% of flow 27. Regarding flow 35, flows 29, 30, 31, 32, 33, 34, and 39 correspond, respectively, to 17.18%, 16.3%, 15.3%, 14.6%, 14.3%, 14.4%, and 9.71%. Furthermore, flows 29, 30, 31, 32, 33, and 34 have temperatures and pressures, respectively, of 346.4 K and 35.8 kPa; 336.8 K and 23.5 kPa; 333.4 K and 20.1 kPa; 330 K and 17.2 kPa; 326.6 K and 14.6 kPa; and 323.2 K and 12.3 kPa.

The total electric power consumption was the sum of the compressors and pump powers, as shown in Eq. (2). The exergy efficiency, Eq. (3), was calculated as the rate of useful exergy at the outlet, corresponding to pure water, divided by the rate of exergy at the inlet, which was the sum of the exergy rate associated with the electric power and to the heat supplied, plus the exergy rate of seawater. Likewise, the exergy efficiency, Eq. (4), was obtained from the overall rate of exergy destruction, Eq. (5), and the total rate of exergy supplied.

$$\dot{W}_{MED} = \dot{W}_{compressorI} + \dot{W}_{compressorII} + \dot{W}_{pumpI} \quad (2)$$

$$\eta_{ex,MED} = 100 \cdot \frac{\dot{B}_{38}}{\dot{B}_{electric} + \dot{B}_1 + \dot{B}_{qIII}} \quad (3)$$

$$\eta_{ex,destroyed,MED} = 100 \cdot \frac{\dot{B}_{electric} + \dot{B}_1 - \dot{B}_{destroyed,MED}}{\dot{B}_{electric} + \dot{B}_1 + \dot{B}_{qIII}} \quad (4)$$

$$\dot{B}_{destroyed,MED} = \dot{B}_{electric} + \dot{B}_1 + \dot{B}_{qIII} - \dot{B}_{38} - \dot{B}_{24} \quad (5)$$

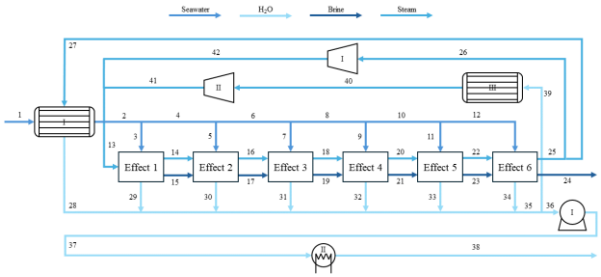

Figure 2. *Schematic representation of Multi-Effect Distillation.*

2.1.2. Reverse Osmosis (RO)

The process considered for reverse osmosis is presented in Figure 3, representing a single-stage plant with energy recovery, based on the work proposed by [37]. A pressure exchanger was selected as the energy recovery device since, compared with energy recovery turbines, it presents higher exergy efficiency and lower exergy destruction [38,39]. Furthermore, the overall and isentropic efficiencies of the pumps were assumed to be 85% and 80%, respectively, while the efficiency of the pressure exchanger was 96%. In addition, the salinity of the seawater was adopted as the standard value of 35 g/kg, and it was assumed that the water enters the system at 298.15 K and 101.325 kPa. It was assumed that the fraction of pure water produced was 40% and that 60% of the inlet water passed through the pressure exchanger. The reverse osmosis membrane module was assumed to operate at 6900 kPa, Pump I increases the pressure in 200 kPa, the brine losing 200 kPa when leaving the module and 100 kPa after the pressure exchanger, and pure water exits at 101.325 kPa.

The total electric power consumption for reverse osmosis was given by the sum of the power of the three pumps, as shown in Eq. (6). The exergy efficiency, given by Eq. (7), was calculated as the rate of useful exergy at the outlet, pure water, divided by the rate of exergy at the inlet, which was the sum of the exergy rate associated with the electric power and the exergy rate of seawater. The exergy efficiency, Eq. (8), was also calculated based on the overall rate of exergy destruction, Eq. (9), and the total rate of exergy supplied.

$$\dot{W}_{RO} = \dot{W}_{pumpI} + \dot{W}_{pumpII} + \dot{W}_{pumpIII} \tag{6}$$

$$\eta_{ex,RO} = 100 \cdot \frac{\dot{B}_9}{\dot{B}_{electric} + \dot{B}_1} \tag{7}$$

$$\eta_{ex,destroyed,RO} = 100 \cdot \frac{\dot{B}_{electric} + \dot{B}_1 - \dot{B}_{destroyed,RO}}{\dot{B}_{electric} + \dot{B}_1} \tag{8}$$

$$\dot{B}_{destroyed,RO} = \dot{B}_{electric} + \dot{B}_1 - \dot{B}_9 - \dot{B}_{11} \tag{9}$$

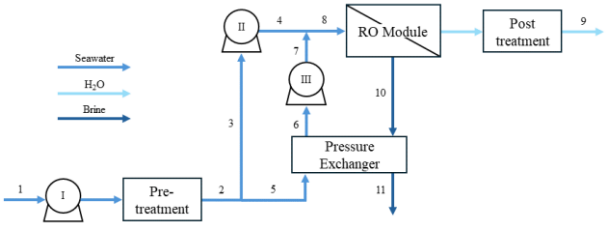

Figure 3. *Schematic representation of Reverse Osmosis, based on* [34].

2.2. Water Electrolysis

Water electrolysis was analyzed considering alkaline (AE), proton exchange membrane (PEM), and solid oxide (SOE) technologies. Alkaline and PEM electrolysis were chosen because they are already commercialized technologies and are widely studied, while SOE is included due to its high efficiency potential associated with operation at high temperatures.

2.2.1. Alkaline Electrolysis (AE)

The alkaline electrolysis plant considered and represented in Figure 4 was developed based on the data presented by [40]. For the calculations, it was assumed that the electrolyzer operates at 700 kPa and 348.15 K, with pump efficiencies of 80%. The KOH electrolyte was 35% by weight in alkaline electrolysis. Separators and heat exchangers had a pressure drop of 30 kPa, while the pumps increased pressure by 60 kPa, except for the first one, which increased the water pressure to 700 kPa. Both the incoming water and the outgoing hydrogen had temperatures of 298.15 K and pressures of 101.325 kPa.

The total power was given by the sum of the power of the pumps, the electrolyzer, and the fan, as shown in Eq. (10). Meanwhile, the exergy efficiency, analyzed in Eq. (11), was calculated by dividing the exergy rate of

hydrogen, since it is the main product of electrolysis, by the inlet exergy rate, which corresponded to the sum of the exergy rate related to the electric power and the exergy rate of the inlet water. The exergy efficiency, defined by Eq. (12), considering the overall exergy destruction rate, described in Eq. (13), and the total exergy rate supplied, was also calculated.

$$\dot{W}_{AE} = \dot{W}_{\text{pump}I} + \dot{W}_{\text{pump}II} + \dot{W}_{\text{pump}III} + \dot{W}_{\text{pump}IV} + \dot{W}_{\text{electrolyzer}} + \dot{W}_{fan} \quad (10)$$

$$\eta_{ex,AE} = 100 \cdot \frac{\dot{B}_{14}}{\dot{B}_{electric} + \dot{B}_1} \quad (11)$$

$$\eta_{ex,destroyed,AE} = 100 \cdot \frac{\dot{B}_{electric} + \dot{B}_1 - \dot{B}_{destroyed,AE}}{\dot{B}_{electric} + \dot{B}_1} \quad (12)$$

$$\dot{B}_{destroyed,AE} = \dot{B}_{electric} + \dot{B}_1 - \dot{B}_{10} - \dot{B}_{11} - \dot{B}_{14} - \dot{B}_{15} \quad (13)$$

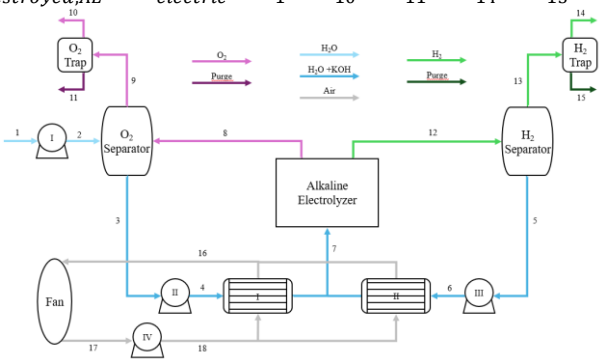

Figure 4. *Schematic representation of Alkaline Electrolysis, based on* [34].

2.2.2. Proton Exchange Membrane Electrolysis (PEM)

In the case of proton exchange membrane electrolysis, Figure 5, the plant proposed by [41] was used as the basis. It was considered that the inlet water and the outlet hydrogen had temperatures of 298.15 K and pressures of 101.325 kPa, that the electrolyzer operated at 353 K and 103.4 kPa and that there was a pressure drop in the heat exchanger of 2.1 kPa.

Equation (14) shows how the total power was calculated, which was the sum of the power of the pumps and the electrolyzer. The exergy efficiency, Eq. (15), resulted from dividing the exergy rate of hydrogen, which is the main product of electrolysis, by the inlet exergy rate, that was the sum of the exergy rate related to the electric power and to the heat supplied, plus the exergy rate of the inlet water. In addition, the exergy efficiency, Eq. (16), was defined using the overall exergy destruction rate, Eq. (17), and the total exergy rate supplied.

$$\dot{W}_{PEM} = \dot{W}_{\text{pump}I} + \dot{W}_{\text{pump}II} + \dot{W}_{\text{pump}III} + \dot{W}_{\text{electrolyzer}} \quad (14)$$

$$\eta_{ex,PEM} = 100 \cdot \frac{\dot{B}_{10}}{\dot{B}_{electric} + \dot{B}_1 + \dot{B}_{qI}} \quad (15)$$

$$\eta_{ex,destroyed,PEM} = 100 \cdot \frac{\dot{B}_{electric} + \dot{B}_1 - \dot{B}_{destroyed,\text{PEM}}}{\dot{B}_{electric} + \dot{B}_1 + \dot{B}_{qI}} \quad (16)$$

$$\dot{B}_{destroyed,PEM} = \dot{B}_{electric} + \dot{B}_1 + \dot{B}_{qI} - \dot{B}_6 - \dot{B}_{10} \quad (17)$$

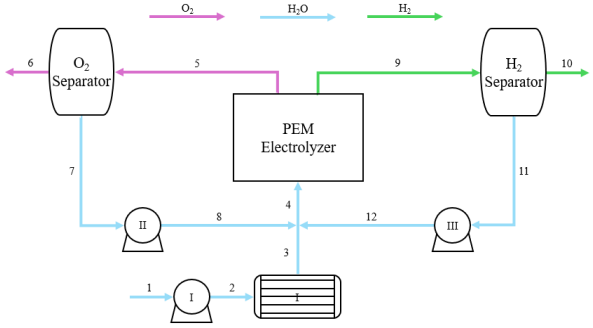

Figure 5. *Schematic representation of Proton Exchange Membrane Electrolysis.*

2.2.3. Solid Oxide Electrolysis (SOE)

Based on the data from [42], the model of the solid oxide electrolysis plant presented in Figure 6 was established. It was assumed that the electrolyzer operated at 890.7 K and 994 kPa, that the conditions of the feed water and the hydrogen at the outlet were 298.15 K and 101.325 kPa, and that the ratio between the total

mass of water in circulation and the feed water flow rate was approximately 2.07. For the separators and heat exchangers II, III, and IV, a pressure drop of 4 kPa was adopted, while for heat exchangers I, V, and VI the pressure drop was 8 kPa.

As presented in Eq. (18), the total electrical power of the system was obtained from the sum of the power consumed by the pump and the power required by the electrolyzer. The exergy efficiency of the process, defined in Eq. (19), was calculated as the ratio between the exergy rate of the hydrogen produced, and the total exergy rate supplied to the system, which corresponds to the sum of the exergy associated with the input electrical energy, heat supplied, and the exergy of the water fed to the process. Additionally, the exergy efficiency based on exergy destruction, as presented in Eq. (20), was determined from the overall exergy destruction rate of the system, shown in Eq. (21), in relation to the total exergy rate supplied.

$$\dot{W}_{SOE} = \dot{W}_{\text{pump}I} + \dot{W}_{\text{electrolyzer}} \tag{18}$$

$$\eta_{ex,SOE} = 100 \cdot \frac{\dot{B}_{21}}{\dot{B}_{electric} + \dot{B}_1 + \dot{B}_{qI} + \dot{B}_{qIV}} \tag{19}$$

$$\eta_{ex,destroyed,SOE} = 100 \cdot \frac{\dot{B}_{electric} + \dot{B}_1 - \dot{B}_{destroyed,SOE}}{\dot{B}_{electric} + \dot{B}_1 + \dot{B}_{qI} + \dot{B}_{qIV}} \tag{20}$$

$$\dot{B}_{destroyed,SOE} = \dot{B}_{electric} + \dot{B}_1 + \dot{B}_{qI} + \dot{B}_{qIV} - \dot{B}_{15} - \dot{B}_{21} \tag{21}$$

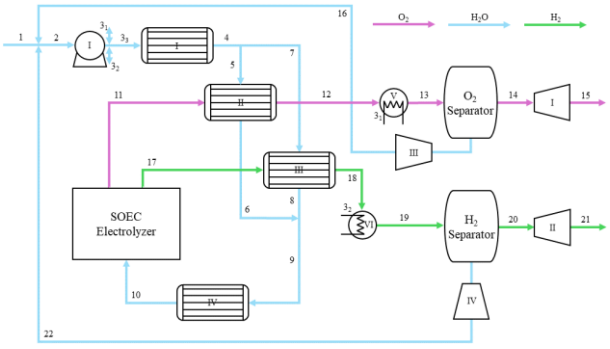

Figure 6. *Schematic representation of Solid Oxide Electrolysis.*

2.3. Nitrogen Extraction

To obtain N_2 from renewable sources, a cryogenic air separation method used by [43] was considered and the developed model is shown in Figure 7. The air is 78.12% N_2, 20.95% O_2, and 0.93% Ar, and its flow was split in a ratio of 85% for the HPC (higher pressure separation column) and 15% for the LPC (lower pressure separation column). From the initial air entering the system, it was assumed that 38.9% of the initial N_2, 18.4% of the Ar, and 75.7% of the O_2 were separated (the purity of O_2 being 98.5%). The thermodynamic parameters, such as the pressures after each compressor, were 198 kPa, 346 kPa, and 635 kPa. The mixture entered the HPC at 570 kPa and 99.35 K, and the LPC at 130 kPa and 79.25 K, 83.65 K, and 82.25 K. Moreover, waste and O_2 were measured at 110 kPa and 298.2 K, N_2 was measured at 101.325 kPa and 298.15 K, while Ar was measured at 120 kPa and 88.85 K.

The total electrical power consumption was given by the sum of the power of the three compressors, as shown in Eq. (22). For the exergy efficiency, Eq. (23) considers in the numerator the useful exergy rate at the outlet, which is the exergy rate of N_2, since this is the component required to produce green ammonia. The denominator was the inlet exergy rate, corresponding to the sum of the exergy rate associated with the electrical power and the exergy rate of the air. In addition, the exergy efficiency, Eq. (24), was calculated considering the overall exergy destruction rate, Eq. (25), and the total exergy rate supplied.

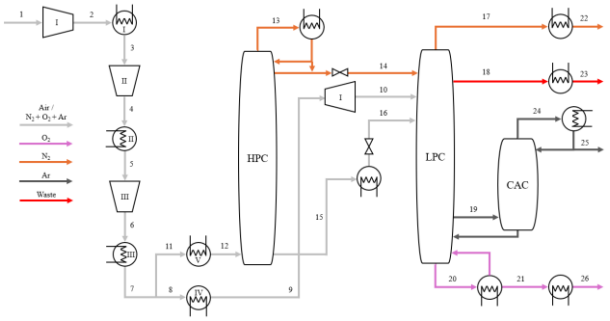

Figure 7. *Schematic representation of Cryogenic Air Separation, based on* [34].

$$\dot{W}_{CAS} = \dot{W}_{compressorI} + \dot{W}_{compressorII} + \dot{W}_{compressorIII} \quad (22)$$

$$\eta_{ex,CAS} = 100 \cdot \frac{\dot{B}_{22}}{\dot{B}_{electric} + \dot{B}_1} \quad (23)$$

$$\eta_{ex,destroyed,CAS} = 100 \cdot \frac{\dot{B}_{electric} + \dot{B}_1 - \dot{B}_{destroyed,CAS}}{\dot{B}_{electric} + \dot{B}_1} \quad (24)$$

$$\dot{B}_{destroyed,CAS} = \dot{B}_{electric} + \dot{B}_1 - \dot{B}_{22} - \dot{B}_{23} - \dot{B}_{25} - \dot{B}_{26} \quad (25)$$

2.4. Ammonia Synthesis

The ammonia synthesis was modeled based on research conducted for large-scale ammonia production by [44,45] and on the study of green ammonia production by [46]. The plant is presented in Figure 8. It was considered that the efficiency of the first reactor was 17.4%, the second 6.1%, and the third 5.7%, while the isentropic efficiency of the compressor was 80%. In addition, the operating pressure of the reactors was 20,000 kPa, with a pressure loss of 130 kPa in the reactors. The operating temperature of the first reactor was 583.15 K, the second 702.45 K, and the third 653.15 K. Furthermore, the percentage of recycled ammonia was 1.81%, and the H_2/N_2 feed ratio to the reactor was 3:1. In addition, hydrogen and nitrogen entered at 101.325 kPa and 298.15 K, while ammonia exited at 101.325 kPa and 239.8 K.

The total electrical power consumption was given by the sum of the power of the compressors, as shown in Eq. (26). The exergy efficiency, Eq. (27), was determined by dividing the useful exergy rate at the outlet, the exergy rate of ammonia, by the inlet exergy rate, which corresponded to the sum of the exergy rate related to the electrical power, the exergy rate of hydrogen, and the exergy rate of nitrogen, plus the exergy rate related to the heat supplied. The exergy efficiency, as represented in Eq. (28), was also determined based on the overall exergy destruction rate, illustrated in Eq. (29), and the total exergy rate supplied.

$$\dot{W}_{HB} = \dot{W}_{compressorI} + \dot{W}_{compressorII} + \dot{W}_{compressorIII} + \dot{W}_{compressorIV} + \dot{W}_{compressorV} \quad (26)$$

$$\eta_{ex,HB} = 100 \cdot \frac{\dot{B}_{15}}{\dot{B}_{electric} + \dot{B}_1 + \dot{B}_{qI}} \quad (27)$$

$$\eta_{ex,destroyed,HB} = 100 \cdot \frac{\dot{B}_{electric} + \dot{B}_1 - \dot{B}_{destroyed,HB}}{\dot{B}_{electric} + \dot{B}_1 + \dot{B}_{qI}} \quad (28)$$

$$\dot{B}_{destroyed,HB} = \dot{B}_{electric} + \dot{B}_1 + \dot{B}_{qI} - \dot{B}_{15} \quad (29)$$

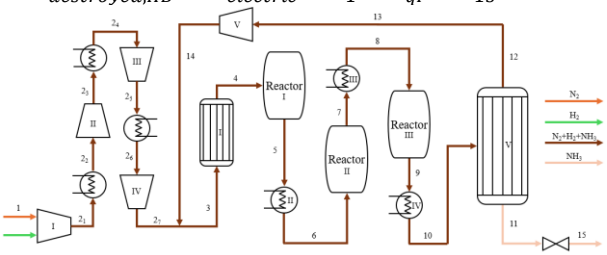

Figure 8. *Schematic representation of Haber-Bosch Synthesis, based on* [34].

3. Results and Discussion

Figures 9, 10 and 11 show the exergy efficiencies, electrical power and destroyed exergy for the processes in the green ammonia production plant. It is observed that, in decreasing order, the efficiencies of the processes were: HB, SOE, AE, PEM, RO, MED, and CAS. Additionally, the exergetic efficiencies calculated based on the rate of exergy destruction followed the same trend observed for the conventional exergetic efficiencies, since the useful products represent the dominant exergy streams in most processes. The main exception was reverse osmosis, which presented the highest exergetic efficiency when calculated based on exergy destruction due to the contribution of the brine stream in the overall exergy balance. Also, the energy consumption and destroyed exergy in increasing order were: RO, MED, CAS, HB, SOE, AE, and PEM.

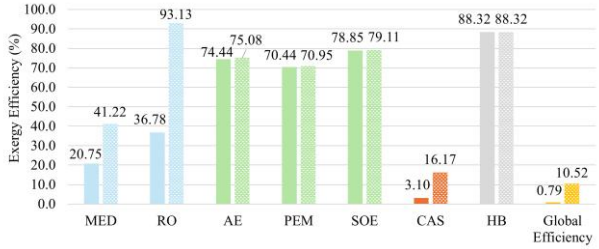

Figure 9. *Results of exergy efficiencies for each process,* η_{ex} *on the left and* $\eta_{ex,destroyed}$ *on the right.*

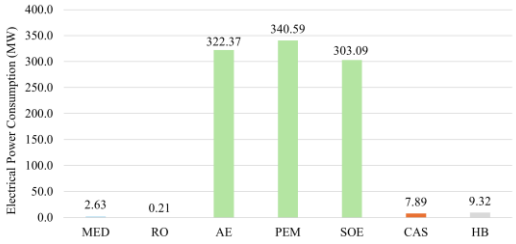

Figure 10. *Results of electrical power consumption for each process.*

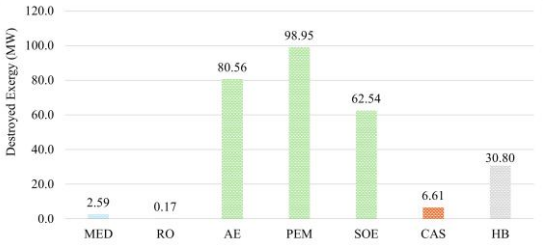

Figure 11. *Results of destroyed exergy for each process.*

For seawater desalination, reverse osmosis achieved $\eta_{ex,RO}$ of 36.78%, close to the literature value of 31.9% [37]. The exergetic efficiency considering the destroyed exergy rate was 93.13%, higher because brine was included. The electrical power required for pure water was 207.1 kW and the destroyed exergy was 0.17 MW. For multi-effect distillation, the exergetic efficiency was 20.75%, very close to literature values of 21.35% [47] and 21.49% [36]. As with RO, the efficiency based on exergy destruction was higher (41.22%) due to the brine stream. The electrical power for MED was 2.63 MW and the destroyed exergy was 2.59 MW.

In electrolysis, alkaline electrolysis showed an exergy efficiency of 74.44%, whereas literature reports lower values (e.g., 55% [48]) due to different operating conditions (lower temperature and electrolyte concentration). The efficiency using the destroyed exergy rate (75.08%) was similar, as other products were negligible. The electrical power was 322.37 MW and the destroyed exergy was 80.56 MW. For PEM electrolysis, both efficiencies were also close (70.44% and 70.95%), in agreement with literature values ranging from 56% to 80% [49–52]. Electrical power was 340.59 MW and the destroyed exergy was 98.95 MW. Solid oxide electrolysis achieved efficiencies of 78.85% and 79.11%, consistent with literature values of 77.62% to 93.11% [42,53], requiring 303.09 MW and the destroyed exergy was 62.54 MW.

Cryogenic air separation considered only N_2 as the useful product for green ammonia, yielding an exergy efficiency of 3.10%, low compared to literature (13% [54] and 14% [43]). However, including oxygen and argon as products raises efficiency to 12.95%, closer to literature. Efficiency based on exergy destruction was 16.17%, higher because all outputs (including waste) are considered. Electrical power required was 7.89 MW and the destroyed exergy was 6.61 MW. For Haber-Bosch synthesis, both efficiencies were 88.32%, within the literature range of 77% to 91.3% [45], requiring 9.32 MW and the destroyed exergy was 30.80 MW.

Thus, from a thermodynamic perspective, reverse osmosis outperforms multi-effect distillation due to lower electrical consumption, higher exergy efficiency, and lower exergy destruction. Among electrolysis methods, SOE stands out with the highest efficiency, followed by AE and then PEM, as reported in the literature [55]. Therefore, the plant with the best performance (highest exergy efficiency, lowest electrical consumption, and lowest exergy destruction) comprised reverse osmosis, SOE electrolysis, cryogenic air separation, and Haber-Bosch synthesis. Overall plant efficiency was 0.79% based on useful products only, and 10.52% based on exergy destruction.

The results highlight the strong influence of the electrolysis stage, since hydrogen production is the most energy-intensive step in green ammonia production, accounting for a large share of total electricity consumption. Thus, improvements in electrolysis efficiency directly impact overall plant efficiency. Although SOE showed higher exergy efficiency, its technological maturity remains lower than that of alkaline and PEM electrolysis, which are commercially available.

Additionally, thermal integration between process units could further improve overall efficiency. It is also important to note that several units within the plant require heat supply. In this context, a question arises: is it consistent with the rational use of energy to employ high-quality electrical energy as a primary input for heat-demanding processes, or should alternative solutions be considered, such as the use of solar thermal exergy or other renewable heat sources? From an exergetic perspective, the use of heat input instead of electrical work, may lead to lower exergy destruction rates, particularly in processes where heat is the main requirement. Furthermore, to ensure that the system can be classified as “green,” it is essential that the energy supplied originates from renewable sources. In this regard, thermal energy can be provided by biomass or biogas-fired

boilers, as well as by solar thermal technologies. Reported efficiencies for these alternatives are relatively high: solar thermal systems may reach efficiencies of up to 70% [56], while biomass boilers can achieve around 85% [57], and biogas-based systems approximately 80% [58].

Despite thermodynamic advantages, the selection of a green ammonia route cannot rely solely on exergy analysis. Each technology has specific advantages and limitations depending on context. For example, RO has lower electricity consumption and higher exergy efficiency, but MED may be advantageous where low-grade waste heat is available or where membrane fouling, chlorine sensitivity, and frequent replacement pose challenges. MED is also robust and suitable for large-scale continuous operation where thermal energy is readily accessible. Although SOE exhibited the highest exergetic efficiency, it faces challenges related to material stability, thermal stresses, and long-term durability, and remains under development for large-scale applications. In contrast, AE is well-established, mature, reliable, safe, and relatively low-cost. PEM offers operational advantages such as high current density, compact design, and rapid response to fluctuating electricity supply, making it suitable for integration with intermittent renewables.

Furthermore, all these technologies are undergoing continuous development, and improvements in efficiency, durability, and cost are expected in the coming years. Therefore, although the configuration combining reverse osmosis and SOE electrolysis presented the best thermodynamic performance in this study, other configurations may be preferable depending on technology maturity, system flexibility, resource availability, and economic considerations.

4. Conclusion

Therefore, the exergy analysis carried out in this study made it possible to evaluate the thermodynamic performance of different technological routes to produce green ammonia from seawater desalination, water electrolysis, cryogenic air separation, and synthesis through the Haber–Bosch process. The results indicated that, among the desalination processes evaluated, reverse osmosis presented higher exergetic efficiency, lower electrical energy consumption and lower exergy destruction when compared with multi-effect distillation. For hydrogen production, solid oxide electrolysis demonstrated the best exergetic performance among the analyzed technologies, followed by alkaline electrolysis and PEM electrolysis. Based on these analyses, it was verified that the configuration composed of RO, SOE electrolysis, CAS, and HB represents the most favorable alternative from a thermodynamic perspective for green ammonia production.

In addition, the results showed that the water electrolysis is responsible for a significant portion of the energy consumption, highlighting it as priority areas for technological improvements and process optimization. Although the identified configuration presents better exergetic performance, the selection of the most suitable route for green ammonia production should also consider factors such as technological maturity, economic feasibility, resource availability, and local operating conditions. Therefore, future studies may explore strategies for energy integration, utilization of waste heat, and techno-economic analyses to further improve the efficiency and feasibility of sustainable ammonia production.

Acknowledgments

The first author is supported by grant 2024/13665-5 FAPESP (São Paulo Research Foundation) and was supported by a CAPES scholarship (Brazilian Federal Agency for Support and Evaluation of Graduate Education). The last author was supported by were supported by the CNPq (the Brazilian National Council for Scientific and Technological Development), grant number 303585/2024-2.

Nomenclature

AE	alkaline electrolysis
b	specific exergy, kJ/kmol
$\dot{B}$	exergy rate, kW
CAS	cryogenic air separation
h	specific enthalpy, kJ/kmol
HB	haber-bosch
MED	multi-effect distillation
$\dot{n}$	molar flow rate, kmol/s
PEM	proton exchange membrane electrolysis
R	universal gas constant, kJ/(kmolK)
RO	reverse osmosis

s specific entropy, kJ/(kmolK)

SOE solid oxide electrolysis

T temperature, K

$\dot{W}$ power, kW

y mole fraction

Greek symbols

η efficiency

Subscripts and superscripts

0 standard

ex exergy

i state

References

[1] Aziz M, Wijayanta AT, Nandiyanto ABD. Ammonia as effective hydrogen storage: A review on production, storage and utilization. Energies (Basel) 2020;13:3062. https://doi.org/10.3390/en13123062.

[2] Ripepi D, Zaffaroni R, Schreuders H, Boshuizen B, Mulder FM. Ammonia Synthesis at Ambient Conditions via Electrochemical Atomic Hydrogen Permeation. ACS Energy Lett 2021;6:3817–23. https://doi.org/10.1021/acsenergylett.1c01568.

[3] Bicer Y, Khalid F. Sustainability assessment of renewable energy-based hydrogen and ammonia pathways. Renewable-Energy-Driven Future, Academic Press; 2021, p. 435–68. https://doi.org/10.1016/B978-0-12-820539-6.00014-5.

[4] Humphreys J, Lan R, Tao S. Development and Recent Progress on Ammonia Synthesis Catalysts for Haber–Bosch Process. Advanced Energy and Sustainability Research 2021;2:2000043. https://doi.org/10.1002/aesr.202000043.

[5] Confederação Nacional da Indústria. OPORTUNIDADES E DESAFIOS PARA GERAÇÃO EÓLICA OFFSHORE NO BRASIL E A PRODUÇÃO DE HIDROGÊNIO DE BAIXO CARBONO. Brasília: CNI; 2023.

[6] Ajanovic A, Sayer M, Haas R. The economics and the environmental benignity of different colors of hydrogen. Int J Hydrogen Energy 2022;47:24136–54. https://doi.org/10.1016/j.ijhydene.2022.02.094.

[7] Zhou Y, Li R, Lv Z, Liu J, Zhou H, Xu C. Green hydrogen: A promising way to the carbon-free society. Chin J Chem Eng 2022;43:2–13. https://doi.org/10.1016/j.cjche.2022.02.001.

[8] Bhandari R, Trudewind CA, Zapp P. Life cycle assessment of hydrogen production via electrolysis - A review. J Clean Prod 2014;85:151–63. https://doi.org/10.1016/j.jclepro.2013.07.048.

[9] Dias BV. ESTUDO DA PRODUÇÃO DE HIDROGÊNIO VIA ELETRÓLISE DO ÁCIDO FÓRMICO. Universidade Estadual do Centro-Oeste, 2016.

[10] El-Shafie M. Hydrogen production by water electrolysis technologies: A review. Results in Engineering 2023;20:101426. https://doi.org/10.1016/j.rineng.2023.101426.

[11] Chisholm G, Zhao T, Cronin L. Hydrogen from water electrolysis. Storing Energy: with Special Reference to Renewable Energy Sources, Elsevier; 2022, p. 559–91. https://doi.org/10.1016/B978-0-12-824510-1.00015-5.

[12] Hermesmann M, Müller TE. Green, Turquoise, Blue, or Grey? Environmentally friendly Hydrogen Production in Transforming Energy Systems. Prog Energy Combust Sci 2022;90:100996. https://doi.org/10.1016/j.pecs.2022.100996.

[13] Dos Santos KG, Eckert CT, De Rossi E, Bariccatti RA, Frigo EP, Lindino CA, et al. Hydrogen production in the electrolysis of water in Brazil, a review. Renewable and Sustainable Energy Reviews 2017;68:563–71. https://doi.org/10.1016/j.rser.2016.09.128.

[14] Saha P, Akash FA, Shovon SM, Monir MU, Ahmed MT, Khan MFH, et al. Grey, blue, and green hydrogen: A comprehensive review of production methods and prospects for zero-emission energy. Int J Green Energy 2024;21:1383–97. https://doi.org/10.1080/15435075.2023.2244583.

[15] Kumar SS, Lim H. An overview of water electrolysis technologies for green hydrogen production. Energy Reports 2022;8:13793–813. https://doi.org/10.1016/j.egyr.2022.10.127.

[16] Da Silva LHO, Conceição ED da, Figueredo MB. Estudo teórico aplicado da Eletrólise para geração de Hidrogênio. REVISTA FOCO 2023;16:e2729–e2729.

[17] Chi J, Yu H. Water electrolysis based on renewable energy for hydrogen production. Chinese Journal of Catalysis 2018;39:390–4. https://doi.org/10.1016/S1872-2067(17)62949-8.

[18] Ramakrishnan S, Delpisheh M, Convery C, Niblett D, Vinothkannan M, Mamlouk M. Offshore green hydrogen production from wind energy: Critical review and perspective. Renewable and Sustainable Energy Reviews 2024;195:114320. https://doi.org/10.1016/j.rser.2024.114320.

[19] Lee B, Wang L, Wang Z, Cooper NJ, Elimelech M. Directing the research agenda on water and energy technologies with process and economic analysis. Energy Environ Sci 2023;16:714–22. https://doi.org/10.1039/d2ee03271f.

[20] Gaio SSM. Produção de água potável por dessalinização: tecnologias, mercado e análise de viabilidade económica. Universidade de Lisboa, 2016.

[21] Torri JB. Dessalinização de água salobra e/ou salgada: métodos, custos e aplicações. Universidade Federal do Rio Grande do Sul, 2015.

[22] Neto JHM. POSSIBILIDADES PARA UTILIZAÇÃO DE PLANTAS HELIOTÉRMICAS PARA GERAÇÃO DE HIDROGÊNIO VERDE VIA ÁGUA DESSALINIZADA, Florianópolis: Anais Congresso Brasileiro de Energia Solar - CBENS; 2022, p. 1–9.

[23] Medeiros VS. Dessalinização de água em uma planta de energia solar concentrada: modelagem e análise termodinâmica. Universidade Federal de Uberlândia, 2021. https://doi.org/10.14393/ufu.di.2021.499.

[24] Júnior JE. A IMPORTÂNCIA DAS TÉCNICAS E USO DA DESSALINIZAÇÃO DA ÁGUA. UNIVERSIDADE FEDERAL RURAL DO SEMIÁRIDO, 2020.

[25] Bovaroti T. AVALIAÇÃO DE UM SISTEMA DE DESSALINIZAÇÃO DE ÁGUA SALOBRA EM ESCALA PILOTO. Universidade Estadual de Ponta Grossa, 2018.

[26] Veerapaneni S, Long B, Freeman S, Bond R. Reducing energy consumption for seawater desalination. Journal-American Water Works Association 2007;99:95–106. https://doi.org/10.1002/j.1551-8833.2007.tb07958.x.

[27] De Oliveira Siqueira AM, Martins ALS, Viana EED. Work principles of different methods of seawater desalination and parametric analysis of a multiple effect desalination (MED). The Journal of Engineering and Exact Sciences 2022;08:13833–01e. https://doi.org/10.18540/jcecvl8iss1pp13833-01-14e.

[28] Busse BAV. Gases Industriais: Simulação do Processo de Separação Criogênica do Ar. Universidade Federal do Rio de Janeiro, 2014.

[29] Zhu Y, Liu X, Zhou Z. Optimization of Cryogenic Air Separation Distillation Columns. 2006 6th World Congress on Intelligent Control and Automation IEEE 2006:7702–5.

[30] Roffel B, Betlem BHL, De Ruijter JAF. First principles dynamic modeling and multivariable control of a cryogenic distillation process. Comput Chem Eng 2000;24:111–23.

[31] Azambuja CM. Modelagem, simulação e análise de eficiência de uma planta de separação de ar. UNIVERSIDADE FEDERAL DO RIO GRANDE DO SUL, 2017.

[32] Espínola MOG. Estudo da viabilidade técnica e econômica do aproveitamento da energia vertida turbinável da Usina Hidrelétrica de Itaipu para a síntese de amônia. UNIVERSIDADE ESTADUAL DE CAMPINAS, 2008.

[33] Dincer I, Zamfirescu C. Sustainable hydrogen production. Elsevier; 2016. https://doi.org/10.1016/b978-0-12-801563-6.00007-8.

[34] Casale IR, Collaço FM de A, Mady CEK. Exergy analysis of hydrogen production aiming at an efficient use of energy for Brazilian society. 38th International Conference on Efficiency, Cost, Optimization, Simulation and Environmental Impact of Energy Systems, Paris: ECOS 2025; 2025.

[35] SZARGUT J. Exergy method: technical and ecological applications. Southampton; Boston: WIT press; 2005.

[36] Dos Santos EBA. Resultados exergéticos, exergoeconômicos e exergoambientais de uma planta de cogeração com microturbina a gás integrada a uma unidade de destilação com múltiplos efeitos. UNIVERSIDADE FEDERAL DO RIO GRANDE DO NORTE, 2023.

[37] Mistry KH, McGovern RK, Thiel GP, Summers EK, Zubair SM, Lienhard JH. Entropy generation analysis of desalination technologies. Entropy 2011;13:1829–64. https://doi.org/10.3390/e13101829.

[38] Eshoul NM, Agnew B, Al-Weshahi MA, Atab MS. Exergy analysis of a two-pass Reverse Osmosis (RO) desalination unit with and without an energy recovery turbine (ERT) and pressure exchanger (PX). Energies (Basel) 2015;8:6910–25. https://doi.org/10.3390/en8076910.

[39] Qureshi BA, Zubair SM. Energy-exergy analysis of seawater reverse osmosis plants. Desalination 2016;385:138–47. https://doi.org/10.1016/j.desal.2016.02.009.

[40] Sánchez M, Amores E, Abad D, Rodríguez L, Clemente-Jul C. Aspen Plus model of an alkaline electrolysis system for hydrogen production. Int J Hydrogen Energy 2020;45:3916–29. https://doi.org/10.1016/j.ijhydene.2019.12.027.

[41] Saray JA, Gharehghani A, Hosseinzadeh D. Towards sustainable energy Carriers: A solar and Wind-Based systems for green liquid hydrogen and ammonia production. Energy Convers Manag 2024;304:118215. https://doi.org/10.1016/j.enconman.2024.118215.

[42] Silva DLI. Design and optimization of hybrid wind-solar energy systems integrated with high-temperature electrolysis for renewable hydrogen production. Universidade de São Paulo, 2025.

[43] Bucsa S, Serban A, Balan MC, Ionita C, Nastase G, Dobre C, et al. Exergetic Analysis of a Cryogenic Air Separation Unit. Entropy 2022;24. https://doi.org/10.3390/e24020272.

[44] Flórez-Orrego D, de Oliveira Junior S. Exergy assessment of single and dual pressure industrial ammonia synthesis units. Energy 2017;141:2540–58. https://doi.org/10.1016/j.energy.2017.06.139.

[45] Flórez-Orrego D, de Oliveira Junior S. Modeling and optimization of an industrial ammonia synthesis unit: An exergy approach. Energy 2017;137:234–50. https://doi.org/10.1016/j.energy.2017.06.157.

[46] Nami H, Hendriksen PV, Frandsen HL. Green ammonia production using current and emerging electrolysis technologies. Renewable and Sustainable Energy Reviews 2024;199. https://doi.org/10.1016/j.rser.2024.114517.

[47] Arakcheeva El Kori N, Blanco-Marigorta AM, Melián Martel N. Definition of Exergetic Efficiency in the Main and Emerging Thermal Desalination Technologies: A Proposal. Water (Basel) 2024;16:1254. https://doi.org/10.3390/w16091254.

[48] Firtina-Ertis I. Thermodynamic and electrochemical assessment of an alkaline electrolyzer (AE) at different operating parameters. J Environ Chem Eng 2022;10. https://doi.org/10.1016/j.jece.2022.107225.

[49] Yilmaz C, Kanoglu M. Thermodynamic evaluation of geothermal energy powered hydrogen production by PEM water electrolysis. Energy 2014;69:592–602. https://doi.org/10.1016/j.energy.2014.03.054.

[50] Yu J, Liu L, Du Y, Li Y, Zhang D, Li B, et al. Thermodynamic and Economic Analysis of the Green Ammonia Synthesis System Driven by Synergistic Hydrogen Production Using Alkaline Water Electrolyzers and Proton Exchange Membrane Electrolyzers. Energy Technology 2024;12:2401169. https://doi.org/10.1002/ente.202401169.

[51] Atiz A, Karakilçik M. Assessment of hydrogen generation and thermodynamic efficiencies of PEM coupled with PV and PV-T under diverse circumstances. Int J Hydrogen Energy 2024;75:132–43. https://doi.org/10.1016/j.ijhydene.2024.01.072.

[52] Badruzzaman A, Karagoz S, Eljack F. Sustainable-green hydrogen production through integrating electrolysis, water treatment and solar energy. Frontiers in Chemical Engineering 2025;7:1526331. https://doi.org/10.3389/fceng.2025.1526331.

[53] AlZahrani AA, Dincer I. Modeling and performance optimization of a solid oxide electrolysis system for hydrogen production. Appl Energy 2018;225:471–85. https://doi.org/10.1016/j.apenergy.2018.04.124.

[54] Açıkkalp E, Yamık H, Caner N, Açıkkalp E. Energy and Exergy Evaluation of an Air Separation Facility: A Case Study. Separation Science and Technology (Philadelphia) 2014;49:2105–13. https://doi.org/10.1080/01496395.2014.907316.

[55] Lima A, Torrubia J, Torres C, Valero A, Valero A. Dynamic small-scale green ammonia non-renewable and renewable exergy costs up to 2050: Short and long-term projections under IEA energy transition scenarios. Renew Energy 2025;256:123891. https://doi.org/10.1016/j.renene.2025.123891.

[56] Mady CEK, Pinto CR, Pereira MTRM. Application of the second law of thermodynamics in Brazilian residential appliances towards a rational use of energy. Entropy 2020;22:616. https://doi.org/10.3390/E22060616.

[57] Compton M, Rezaie B. Sustainability Enhancement of a Biomass Boiler through Exergy Analysis, MDPI AG; 2017, p. 159. https://doi.org/10.3390/ecea-4-05012.

[58] Saka K. A Quantitative Examination of the Efficiency of a Biogas-Based Cooling System in Rural Regions. Processes 2023;11:1983. https://doi.org/10.3390/pr11071983.